Protoplasma (2019) 256:1145–1151
https://doi.org/10.1007/s00709-019-01371-5

ORIGINAL ARTICLE

Mesopore structure in *Camellia Oleifera* shell

Qianqian Wang[1] · Shanshan Chang[1] · Yujing Tan[1] · Jinbo Hu[1]

Received: 28 January 2019 / Accepted: 21 March 2019 / Published online: 5 April 2019

Abstract

Generally, *Camellia oleifera* shells are byproducts of edible oil production and are often incinerated or discarded as agricultural waste without any sustainable uses. Although numerous studies have focused on the *C. oleifera* shell, few studies have examined its biological characteristics, particularly its internal mesoporosity. The aim of the present study was to elucidate the microscopic biological structure of *C. oleifera* shells to explore their potential applications. Paraffin-embedded slices of *C. oleifera* shells were observed on different planes using an optical microscope. Supercritically dried samples were prepared and assessed using the nitrogen adsorption-desorption technique to reveal mesopore structural features. The present article shows that *C. oleifera* shells were mainly made up of stone cells, parenchyma tissue, spiral vessels, and vascular bundles. The key features of the cells were the pits in the cell walls of stone cells and vessels, which are associated with the abundant mesopores in *C. oleifera* shells. *C. oleifera* shells have an advantage over woody materials based on their mesoporosity features. *C. oleifera* shells are ideal raw materials that could serve as biomass templates or find applications as other high-performance biomimetic materials.

Keywords Camellia oleifera shell · Stone cell · Mesopore · Nitrogen adsorption

Introduction

Camellia oleifera is a woody species found in China, which produces edible oil. Forest areas with *C. oleifera* in China consist of 18 key areas, mainly in Hunan, Jiangxi, and Guangxi (Xiong et al. 2007; Liu et al. 2018a). *C. oleifera* is a valuable resource. Its fruits, which are composed of seeds and shells, are mainly exploited as a source of high-quality edible oil. However, the shells are generally byproducts of oil production activities and are regarded as agricultural waste. The shells are yet to find sustainable applications. The shells account for approximately 50–60% of the total weight of the whole fruit. During the oil production process, 1 ton of *C. oleifera* fruits produces 0.54 tons of shells (Zhu et al. 2013; Hu et al. 2015). Therefore, *C. oleifera* shells represent a rich biomass resource. However, the shells are often burned or simply discarded.

The major components of *C. oleifera* shells are cellulose, hemicellulose, and lignin, which are also the major components of wood (Peng et al. 2016). Recently, the components of *C. oleifera* shell have been used to produce furfural, xylitol, tannin, and culture media (Jin 2012; Zhang et al. 2017; Xie et al. 2018). In addition, based on the natural properties of *C. oleifera* biomass, the shells have been extensively used in the manufacture of activated carbon (Kang et al. 2011; Li et al. 2016). Although most studies have focused on the composition of the *C. oleifera* shell, relatively few studies have explored its natural microstructure, particularly its internal pore structure. To exploit the *C. oleifera* shell sustainably, it is necessary to understand its basic microstructural characteristics. In the present study, fresh *C. oleifera* shells were observed from three planes with the aim of clarifying the cell structure types. The mesoporous structures of supercritical dried *C. oleifera* shell samples were analyzed and characterized using the nitrogen sorption isotherm technique. Basic information on the biological structure could facilitate the determination of its potential uses.

Handling Editor: Peter Nick

Electronic supplementary material The online version of this article (https://doi.org/10.1007/s00709-019-01371-5) contains supplementary material, which is available to authorized users.

✉ Shanshan Chang
changelxy@hotmail.com

✉ Jinbo Hu
hjb1999@hotmail.com

[1] College of Material Science and Engineering, Central South University of Forestry and Technology, Changsha 410004, People's Republic of China

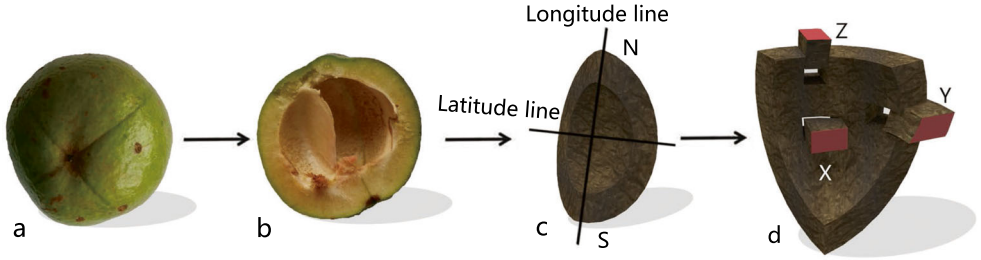

Fig. 1 *C. oleifera* fruit and sample observation planes diagram. **a** Fresh *C. oleifera* fruit. **b** Longitudinally dissected *C. oleifera* fruit without seeds. **c** Diagram of the longitudinal and latitudinal directions of *C. oleifera* shell. **d** Diagram of the three observation sections (X, Y, Z) of *C. oleifera* shell. N north pole, S south pole

Materials and methods

Materials

Fresh *C. oleifera* fruits grown in Changsha, at the Chinese National Engineering Research Center for Olitea Camellia, in central south China were sampled on 29 October 2017 during the mature stages (Fig. 1a). The sample fruits were uniform in size and color and had not been attacked by insects. After being cleaned, the selected samples were cut longitudinally (Fig. 1b). The seeds were extracted from the fruits carefully to avoid damaging the endocarp, and the shells were maintained under wet conditions during sampling. The shells were stored in FAA fixative solution (38% formaldehyde, glacial acetic acid, and 70% alcohol at a 5:5:90 volume ratio) to maintain the original cell morphology of the shells.

The shells were divided on two planes to facilitate better distinction of the observed shell surfaces. As illustrated in Fig. 1c, a longitudinal cut was made from the top (north pole) to the pedicel (south pole), and a latitudinal cut was made perpendicular to the longitudinal line. Three sections, named as X, Y, and Z, were used to investigate the microstructure of the *C. oleifera* shells (Fig. 1d). The X section represented the observation plane from the endocarp to the exocarp side following seed removal. The Y section represented the observation plane obtained by cutting along the longitudinal line, while the Z section represented the observation plane obtained by cutting along the latitudinal line.

Microscopic observation

Three blocks (X, Y, and Z) obtained from one *C. oleifera* shell were dehydrated with ethanol and embedded in paraffin. Ten-micrometer-thick sections were cut using a HM325 rotary microtome (Thermo Fisher Scientific), stained with fast green FCF (AR, Sigma-Alorigh) and safranin O (AR, Ourchem), and observed under an optical microscope (Nikon H550S). In addition, three sections (X, Y, and Z) of supercritically dried *C. oleifera* shell samples were observed under a scanning electron microscope (SEM, Quanta 450) after platinum metallization.

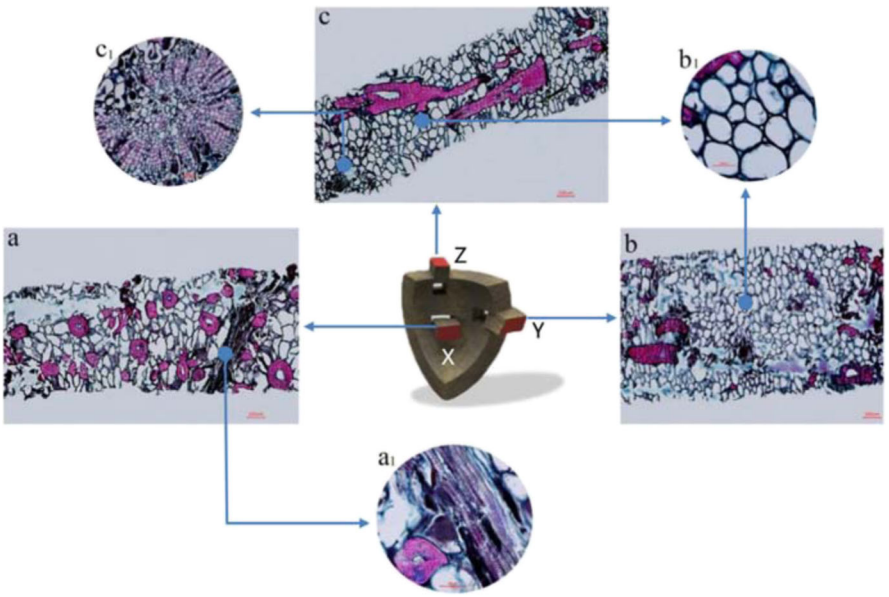

Fig. 2 The microstructure (a, b, and c) of *C. oleifera* shell in three observation planes. a_1 Enlarged view of vascular tissue. b_1 Enlarged view of parenchyma. c_1 Enlarged view of spiral vessel and stone cell. Scale bars in a, b, and c = 100 μm, scale bars in a_1, b_1, and c_1 = 40 μm

Fig. 3 The magnified view of stone cells in three observation planes. **a**–**c** The views from X, Y, and Z sections separately. Scale bars in **a**, **b**, and **c** = 40 μm

Supercritical drying

Before nitrogen adsorption-desorption measurements, the samples had to be supercritically dried to maintain the integrity of the internal pore structures (Clair et al. 2008). Immediately after sampling, samples (2 × 2 × 2 mm) were kept in 30% ethanol and dehydrated in an ethanol series (50%, 70%, 85%, 95%, and 100% three times) for a total of 24 h. The dehydrated samples were then introduced into a K850 critical point drier with liquid CO_2 as the transitional fluid and supercritically dried with a null surface tension.

Nitrogen adsorption-desorption measurement

Nitrogen adsorption-desorption measurements were carried out on a Coulter SA3100 apparatus (Coulter Corporation) at 77 K. Prior to the adsorption experiment, the supercritically dried samples (sample weights were preferably between 0.15 g and 0.25 g) were outgassed at 323 K in a vacuum until a static 3×10^{-5} Torr pressure was reached to eliminate the physically adsorbed gases from the sample surfaces, particularly water vapor. The experimental technique facilitates the measurement of the adsorption-desorption isotherms, surface area (S_{BET}, Brunauer et al. 1938), pore volume (Gregg and Sing 1982), and pore size distribution (Broekhoff and de Boer 1967) in the samples.

Results

Microstructure observation

Figure 2 shows the microscopic structures of three sections (X, Y, and Z) of *C. oleifera*. Four major types of tissues were observed, including stone cells (Figs. 2 (a_1) and 3), vessels (Fig. 2 (a_1)), parenchyma (Figs. 2 (b_1)), and vascular tissue (Figs. 2 (c_1)), which are largely consistent with the results of Hu et al. (2018) except for vascular tissue. Parenchyma cells were mostly elliptical or irregular and had thin walls and large lumen, appearing abundant in all three directions. Some nutrient substances visible in the cell lumen highlighted the critical storage functions of the cells. Unlike other woody materials, vessels in *C. oleifera* shells exist in clusters with spirally thickened walls. The function of a spiral vessel is to transport nutrients and moisture, being observed mostly in groups of strips in the X and Y directions and do not exist independently. Vascular tissues generally consist of a powerful transmission and support system consisting of phloem, xylem, and fascicular cambium, separately, with the shape of a cluster surrounded by parenchyma in the Z direction. Vascular tissues are mainly composed of thick-walled cells, with regular rectangular shapes at the cell edges.

Stone cells were easily distinguished by a red color (Figs. 2 (a_1) and 3) following safranin O staining. Compared to other cell types, stone cells had much thicker cell walls and had small cell lumen. Since the thick walls play a mechanical and protective role in the shells, stone cells may also exist in plant organs such as fruits and seeds, which are formed by the deposition of lignin on primary cell walls (Jin et al. 2013), followed by the secondary thickening of cell walls. Abundant pits were visible in the stone cell walls, and they provided pathways for substance exchange between cells. Most stone cells were scattered and exhibited different shapes in three directions (Fig. 3). Table 1 summarizes the morphology of stone cells observed on different planes. From Fig. 3 and Table 1, it can be inferred that the shapes of the stone cells are irregular and could be long cylindrical structures or spherical. From the X section

Table 1 The morphology of stone cells in different observation directions

Sections	Morphology of stone cells
X	The round shapes with thicker cell wall and small cell lumen are dominant, supplemented long and irregular shapes
Y	Long and irregular shapes are dominant and smaller circular are scattered
Z	Long and irregular shapes, as well as irregular shape with small size distributions, each accounting for half the amount

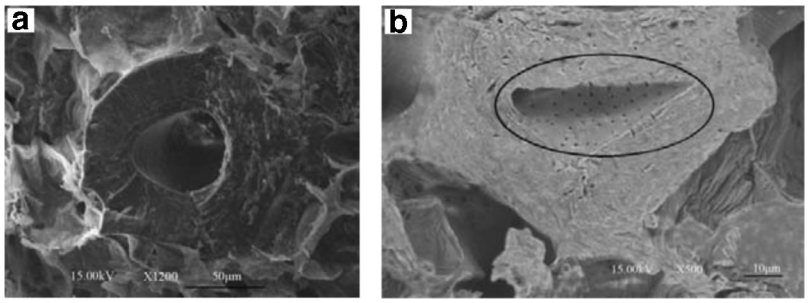

Fig. 4 The SEM observation of stone cells in *C. oleifera* shell scale bars in **a** = 50 μm, scale bars in **b** = 30 μm. Black ellipse: pits in the thick wall stone cell

(Fig. 3a), the stone cells were either oval or spherical with interpenetrating pore structures surrounding the cell walls. However, in the Y and Z sections, stone cells had largely irregular spindle-like shapes with occasional circular shapes. Plurality of pits could be observed in the X, Y, and Z sections; with obvious pore structures under SEM observation (Fig. 4).

Analysis of adsorption-desorption isotherm

From Fig. 5, the N_2 adsorption-desorption isotherm of *C. oleifera* shell is irreversible and can be classified into II and IV(b) mixed type with H2(b) and H3 hysteresis loop, according to the International union of pure and applied chemistry (IUPAC) classification system (Thommes et al. 2015).

At the lower relative pressure stage ($0 < p/p^0 < 0.1$), the adsorption curve rises more rapidly and was concave to the relative pressure p/p^0 axis, indicating that the micropores of *C. oleifera* shell filling at this stage. As pressure increases, a sharp knee-bend is generally observed in the isotherm, indicating that the saturation amount of the single-layer adsorption starts to overlap with the initial amount of the multilayer adsorption (Kuila and Prasad 2013). At the medium pressure stage ($0.2 < p^0 < 0.8$), the curve still rose gradually. With increase in pressure ($0.8 < p/p^0 < 1.0$), the adsorption isotherm rose more rapidly than previously, indicating that multilayer adsorption occurred at the stage, mainly corresponding to the filling of mesopores and macropores. When the relative pressure p/p^0 was close to 1, the adsorption isotherm was almost parallel to the y axis and did not appear on the platform. That is, the adsorption was not saturated, indicating that there was a certain amount of macropores. The desorption branch was not reversible, with the adsorption branch showing a steep decline at a relative pressure p/p^0 0.5. When the relative pressure p/p^0 was less than 0.4, the desorption isotherm was almost coincident with the adsorption isotherm.

The type of hysteresis loop could offer information about mesopore shape in *C. oleifera* shells. According to the IUPAC classification system (Thommes et al. 2015), the hysteresis loop is intermediate between type H2(b) and type H3, indicating the presence of ink-bottle pores with a non-uniform size and layered-slit pores with a broad size distribution, which extends to the macropore domain. At a p/p^0 of approximately 0.5, the hysteresis loop has a distinct inflection point due to the size difference between ink-bottle pore throat and

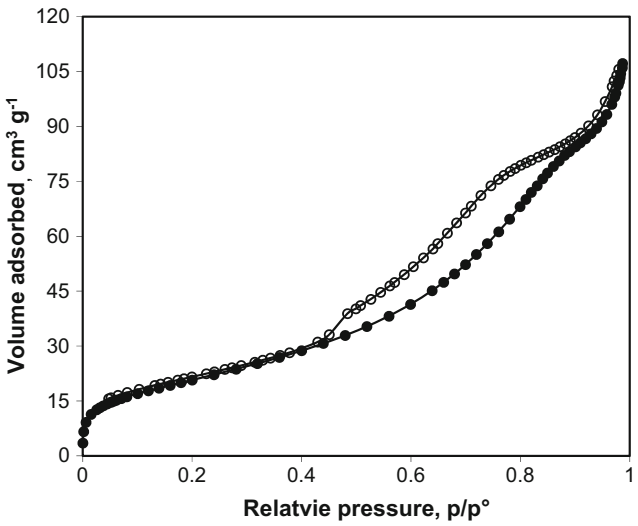

Fig. 5 N_2 adsorption-desorption at 77 K isotherm of *C. oleifera* shell

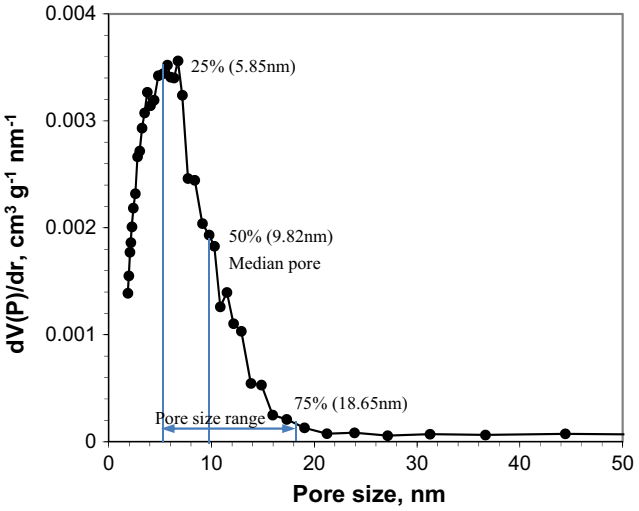

Fig. 6 Pore size distribution of *C. oleifera* shell. The three vertical lines represent the pore sizes at 25%, 50%, and 75% of the pore volume

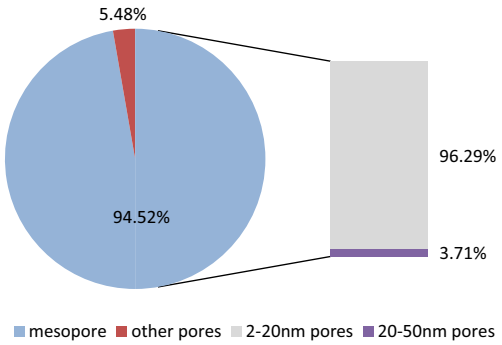

Fig. 7 Specific surface area ratio of different pore size region

stomach, and the relative pressure required for the evaporation of adsorbate is different.

Pore size distribution

The Broekhoff and de Boer (1967) method was used to determine pore size distributions, and it was demonstrated to be more accurate than the commonly used Barrett-Joyner-Halenda (BJH) method (Barrett et al. 1951; Galarneau et al. 1999). The adsorption branch was used for pore size distribution (Fig. 6) to avoid the influence of the false peak near 4 nm in the desorption curve. Majority of the accessible pores exhibited diameters between 2 and 50 nm, with the peak in the pore size distribution curve occurring at a diameter of 9 nm. In order to characterize the overall distribution of pore size, pore sizes were characterized not only based on peak pore size but also based on their distribution ranges, which were calculated from the adsorption pore size distribution diagram (Fig. 6) after integration of the area under the curve of pore size distribution (Chang et al. 2015). The median pore size (at 50% of the pore volume) was approximately 10 nm with pore size ranging from 6 nm to 18 nm.

Pore surface area and pore volume

Based on the measurements, the specific surface area (S_{BET}) of *C. oleifera* shell was 76.22 $m^2 \cdot g^{-1}$. The compound pie chart ratio diagram of S_{BET} (Fig. 7) indicates that the mesopore surface area accounts for 94.52% of the total specific surface area. The S_{BET} of pore size ranging between 2 nm and 20 nm were the majority and accounted for 96.29% of the mesopore surface area. The pore volume data were strongly correlated with the surface area. Similar to the distribution characteristics of pore surface area, the mesopore pore volume accounted for 87.50% of the total pore volume, which was 0.16 ml g^{-1}. In the mesoporous pores, 85.70% of pore volumes were associated with pore sizes ranging between 2 nm and 20 nm.

Discussion

Observation under a microscope revealed that mature *C. oleifera* shells mainly consisted of stone cells, parenchyma tissue, vessels, and vascular bundles. Among the cell types, the stone cells and parenchyma tissue were predominant and accounted for almost 90% of the total cell tissues. In *C. oleifera* shells, stone cells function as mechanical tissue with thick cell walls and narrow cell lumen. The wall thickness-to-cavity ratio of stone cells is approximately 10, up to a maximum of 17. Abundant pits on the thick wall provide the transport channels for nutrition across cells, and it also provides the basis for potential biomass applications, since the mesoporosity of *C. oleifera* shells has been demonstrated through nitrogen adsorption-desorption technique. Pore sizes

Table 2 S_{BET} of *C. oleifrea* shell compared to several lignocellulosic materials from literature

Biomass material	S_{BET}($m^2 \cdot g^{-1}$)	Literature sources
C. oleifera shell	76.22	
Corsican pine	6.63	Papadopoulos et al. (2003)
Scots pine	5.93	
Castanea sativa Mill	0.56 (normal wood)	Clair et al. (2008)
	18.80(tensin wood)	
Polpar (*Populus* sp.)	1.70 (normal wood)	Chang et al. (2011)
	26 (tensin wood)	
Isolated gelatinous layers from poplar (*Populus deltoides* × *P. nigra*)	35 (tension wood)	Chang et al. (2017)
Cambium zone in poplar (*Populus deltoides* (Battr) Marsh × *P. nigra* L)	153 (normal wood)	Chang et al. (2015)
	180 (tension wood)	
Moso bamboo	82.04	He et al. (2017)

between 2 nm to 20 nm represent majority of the total pore volume and pore surface area, exhibiting ink-bottle or layered-slit pore shapes. The similar mesopore structure has also been observed in other woody species, but it is more abundant in *C. oleifera* shell. For example, the specific surface area, S_{BET}, of a *C. oleifera* shell was compared with that in wood, bamboo, and cell walls or cambium zones in wood material-based literature (Table 2). *C. oleifera* shell exhibits the relatively excellent pore structure, comparable to moso bamboo, and the S_{BET} value is much higher than that in softwood, hardwood, and in the gelatinous layer of poplar tension wood, but much lower than that in the cambium zone in poplar wood, which has high amounts of mesopores existing in pectin (Chang et al. 2015). The mesoporous structure in *C. oleifera* shell is an adaptation to the environment during plant growth. The mesoporous structure also makes the *C. oleifera* shell suggests that it could have biomass applications similar to other nutshell materials, e.g., oil palm shell (Hoseinzadeh Hesas et al. 2015), coconut shell (Achaw and Afrane 2008; Li et al. 2008), and peanut shell (Liu et al. 2018b). Biomass-based porous materials have more and superior application prospects in the fields of medicine, energy, and electrochemistry. Using the pore structure of natural biomass as a template for preparing adsorbents, carriers, and supercapacitor electrodes has been widely applied in recent years (Thambidurai et al. 2014; Adinaveen et al. 2015; Alabadi et al. 2015).

Conclusion

The anatomy and mesopore structure of *C. oleifera* shells were studied in the present study. The mesoporosity of *C. oleifera* shells was measured using the nitrogen adsorption-desorption technique, which was largely facilitated to the integrity of pit membranes of stone cells or cavities between macrofibrils in the cell wall. In *C. oleifera* shells, pore sizes ranging between 2 nm and 20 nm were the majority, which suggested their advantages over solid woody materials. The natural microstructural features of *C. oleifera* shells suggest that the agro-waste could be sustainably managed and offers a biological basis for applications such as targeted preparation of high-performance biomimetic materials and, in addition to providing biomass templates.

Acknowledgments We thank Chinese National Engineering Research Center for Olitea Camellia, Changsha, P.R. China, for assisting us during the field sampling.

Authors' contributions Conceived and designed the experiments: QW, SC, JH; performed the experiment: QW, YT; supervised the work: SC, JH; wrote the paper: QW, SC, JH; revised the paper: QW, SC, JH.

Funding information This work was financially supported by the Hunan Provincial Natural Science Foundation of China (2017JJ1038).

Compliance with ethical standards

Ethics approval and consent to participate Ethics approval and consent to participate are not applicable in this study.

Conflict of interest The authors declare that they have no conflict of interest.

References

Achaw OW, Afrane G (2008) The evolution of the pore structure of coconut shells during the preparation of coconut shell-based activated carbons. Microporous Mesoporous Mater 112:284–290. https://doi.org/10.1016/j.micromeso.2007.10.001

Adinaveen T, John Kennedy L, Judith Vijaya J, Sekaran G (2015) Surface and porous characterization of activated carbon prepared from pyrolysis of biomass (rice straw) by two-stage procedure and its applications in supercapacitor electrodes. J Mater Cycles Waste Manag 4: 736–147. https://doi.org/10.1007/s10163-014-0302-6

Alabadi A, Razzaque S, Yang Y, Chen S, Tan B (2015) Highly porous activated carbon materials from carbonized biomass with high CO2 capturing capacity. Chem Eng J 281:606–612. https://doi.org/10.1016/j.cej.2015.06.032

Barrett E, Joyner L, Halenda P (1951) The determination of pore volume and area distributions in porous substances. I. Computations from nitrogen isotherms. J Am Chem Soc 73:373–380. https://doi.org/10.1021/ja01145a126

Broekhoff JCP, de Boer JH (1967) Studies on pore systems in catalysts: XIII. Pore distributions from the desorption branch of a nitrogen sorption isotherm in the case of cylindrical pores B. Applications. J Catal 9:8–14. https://doi.org/10.1016/0021-9517(67)90174-1

Brunauer S, Emmett PH, Teller E (1938) Adsorption of gases in multimolecular layers. J Am Chem Soc 60:309–319. https://doi.org/10.1021/ja01269a023

Chang S, Hu J, Clair B, Quignard F (2011) Pore structure characterization of poplar tension wood by nitrogen adsorption-desorption method. Sci Silvae Sin 47:134–140. https://doi.org/10.11707/j.1001-7488.20111021

Chang S, Quignard F, Alméras T, Clair B (2015) Mesoporosity changes from cambium to mature tension wood: a new step toward the understanding of maturation stress generation in trees. New Phytol 205:1277–1287. https://doi.org/10.1111/nph.13126

Chang S, Quignard F, Clair B (2017) The effect of sectioning and ultrasonication on the mesoporosity of poplar tension wood. Wood Sci Technol 51:507–516. https://doi.org/10.1007/s00226-017-0890-0

Clair B, Gril J, Di Renzo F, Yamamoto H, Quignard F (2008) Characterization of a gel in the cell wall to elucidate the paradoxical shrinkage of tension wood. Biomacromolecules 9:494–498. https://doi.org/10.1021/bm700987q

Galarneau A, Desplantier D, Dutartre R, Di Renzo F (1999) Micelle-templated silicates as a test-bed for methods of pore size evaluation. Microporous Mesoporous Mater 27:297–308. https://doi.org/10.1016/S1387-1811(98)00263-7

Gregg SJ, Sing KSW (1982) Adsorption, surface area and porosity. Academic Press, London

He S, Xu J, Wu z BY, Yu H, Chen Y (2017) Compare of porous structure of moso bamboo and *Pinus sylvestris* L. lumber. J Nanjing Forestry Univ 41:157–162. https://doi.org/10.3969/j.issn.1000-2006.2017.02.023

Hoseinzadeh Hesas R, Arami-Niya A, Wan Daud WMA, Sahu JN (2015) Microwave-assisted production of activated carbons from oil palm shell in the presence of CO2 or N2 for CO2 adsorption. J Ind Eng Chem 24:196–205. https://doi.org/10.1016/j.jiec.2014.09.029

Hu J, Chang S, Peng K, Hu K, Thevenon MF (2015) Bio-susceptibility of shells of *Camellia oleifera* Abel. fruits to fungi and termites. Int Biodeterior Biodegrad 104:219–223. https://doi.org/10.1016/j.ibiod.2015.06.011

Hu J, Shi Y, Liu Y, Chang S (2018) Anatomical structure of *Camellia oleifera* shell. Protoplasma 6:1777–1784. https://doi.org/10.1007/s00709-018-1271-8

Jin X (2012) Bioactivities of water-soluble polysaccharides from fruit shell of *Camellia oleifera* Abel: antitumor and antioxidant activities. Carbohydr Polym 87:2198–2201. https://doi.org/10.1016/j.carbpol.2011.10.047

Jin Q, Yan C, Qiu J, Zhang N, Cai Y (2013) Structural characterization and deposition of stone cell lignin in Dangshan Su pear. Sci Hortic-Amsterdam 155:123–130. https://doi.org/10.1016/j.scienta.2013.03.020

Kang S, Jianchun J, Dandan C (2011) Preparation of activated carbon with highly developed mesoporous structure from *Camellia oleifera* shell through water vapor gasification and phosphoric acid modification. Biomass Bioenergy 35:3643–3647. https://doi.org/10.1016/j.biombioe.2011.05.007

Kuila U, Prasad M (2013) Specific surface area and pore-size distribution in clays and shales. Geophys Prospect 61:341–362. https://doi.org/10.1111/1365-2478.12028

Li W, Yang K, Peng J, Zhang L, Guo S, Xia H (2008) Effects of carbonization temperatures on characteristics of porosity in coconut shell chars and activated carbons derived from carbonized coconut shell chars. Ind Crop Prod 28:190–198. https://doi.org/10.1016/j.indcrop.2008.02.012

Li K, Liu S, Shu T, Yan L, Guo H, Dai Y, Luo X, Luo S (2016) Fabrication of carbon microspheres with controllable porous structure by using waste *Camellia oleifera* shells. Mater Chem Phys 181:518–528. https://doi.org/10.1016/j.matchemphys.2016.06.089

Liu C, Chen L, Tang W, Peng S, Li M, Deng N, Chen Z (2018a) Predicting potential distribution and evaluating suitable soil condition of oil tea camellia in China. Forests 9:487. https://doi.org/10.3390/f9080487

Liu J, Liu Y, Peng J, Liu Z, Jiang Y, Meng M, Zhang W, Ni L (2018b) Preparation of high surface area oxidized activated carbon from peanut shell and application for the removal of organic pollutants and heavy metal ions. Water Air Soil Pollut 229:391. https://doi.org/10.1007/s11270-018-4021-9

Papadopoulos AN, Hill CAS, Gkaraveli A (2003) Determination of surface area and pore volume of holocellulose and chemically modified wood flour using the nitrogen adsorption technique. Holz Roh Werkst 61:453–456. https://doi.org/10.1007/s00107-003-0430-5

Peng K, Hu J, Chen G, Hu K, Ma X (2016) Research of chemical composition and combustion performance of *Camellia oleifera* fruit shells. J Cent South Univ Forestry Technol 36:123–128. https://doi.org/10.14067/j.cnki.1673-923x.2016.07.021

Thambidurai A, Lourdusamy JK, John JV, Ganesan S (2014) Preparation and electrochemical behaviour of biomass based porous carbons as electrodes for supercapacitors—a comparative investigation. Korean J Chem Eng 31:268–275. https://doi.org/10.1007/s11814-013-0228-z

Thommes M, Kaneko K, Neimark AV, James PO, Francisco RR, Jean R, Kenneth SWS (2015) Physisorption of gases, with special reference to the evaluation of surface area and pore size distribution (IUPAC technical report). Pure Appl Chem 87. https://doi.org/10.1515/ci-2016-0119

Xie Y, Ge S, Jiang S, Liu Z, Chen L, Wang L, Chen J, Qin L, Peng W (2018) Biomolecules in extractives of *Camellia oleifera* fruit shell by GC-MS. Saudi J Biol Sci 25:234–236. https://doi.org/10.1016/j.sjbs.2017.08.006

Xiong W, Fu JP, Wang HB, Han XD, lei W (2007) Secondary metabolites from the fruit shells of *Camellia oleifera*. Chem Nat Compd 54:1189–1191. https://doi.org/10.1007/s10600-018-2592-8

Zhang L, He Y, Zhu Y, Liu Y, Wang X (2017) *Camellia oleifera* shell as an alternative feedstock for furfural production using a high surface acidity solid acid catalyst. Bioresour Technol 249:536–541. https://doi.org/10.1016/j.biortech.2017.10.061

Zhu J, Zhu Y, Jiang F, Ouyang J, Yu S (2013) An integrated process to produce ethanol, vanillin, and xylooligosaccharides from *Camellia oleifera* shell. Carbohydr Res 382:52–57. https://doi.org/10.1016/j.carres.2013.10.007